Passive Regenerative and Dissipative Snubber Cells for Isolated SEPIC Converters: Analysis, Design, and Comparison

Gabriel Tibola, *Member, IEEE*, Erik Lemmen, *Student Member, IEEE*, Jorge L. Duarte, *Member, IEEE*, and Ivo Barbi, *Fellow, IEEE*

***Abstract*—An isolated converter such as SEPIC has high voltage stress on the main switch due to transformer leakage inductance. To solve this issue, active or passive clamp action is necessary. The common passive solution based on an RCD snubber is simple but impractical when the value of the leakage inductance is significant. On the other hand, passive regenerative solutions generally compromise the isolation, making the search for a suitable snubber a challenge. In this paper, an effective passive regenerative snubber cell for isolated SEPIC converters operating in DCM or CCM is presented. It is intended to improve the converter efficiency by transferring the energy stored in the transformer leakage inductance to the output. The analysis is presented in detail for DCM and extended to CCM together with a practical design procedure. In order to compare with the RCD, the analysis and design of a conventional cell are presented as well. To validate the proposal and quantify its feasibility, experimental results are performed for both dissipative and regenerative snubbers on a 100 W, 100 V, input and 50 V output voltage converter operating first in DCM and later in CCM.**

***Index Terms*—RCD snubber, regenerative snubber, SEPIC converter.**

I. Introduction

SINGLE ended primary inductance converter (SEPIC) is one of the basic power electronic topologies. It can be used in a variety of applications, such as switched mode power supplies and power factor correction units. Examples are well known in single-phase [1]–[3] or three-phase [4], [5] applications. This converter has some advantages when compared to other conventional topologies, such as the continuous low ripple current at the input for any operational mode. Moreover, the SEPIC can operate as a step-up or step-down converter and has the possibility to provide one or more isolated outputs.

Although, when isolation is required, the voltage stress across the main switch, which is equal to the input voltage V_i plus the output voltage V_o referred to the transformer (T) primary side by a relation n, becomes larger. This happens since the energy stored in the transformer leakage inductance has no path to circulate, causing voltage spikes across the main switch. Fig. 1(a) shows the isolated version of the SEPIC, including the leakage inductance L_k and magnetizing inductance L_o, referred to the transformer primary side.

Due to voltage spikes, a snubber is required to prevent damage to the switch. Two approaches are commonly found in the literature, the passive dissipative or regenerative snubbers, and the

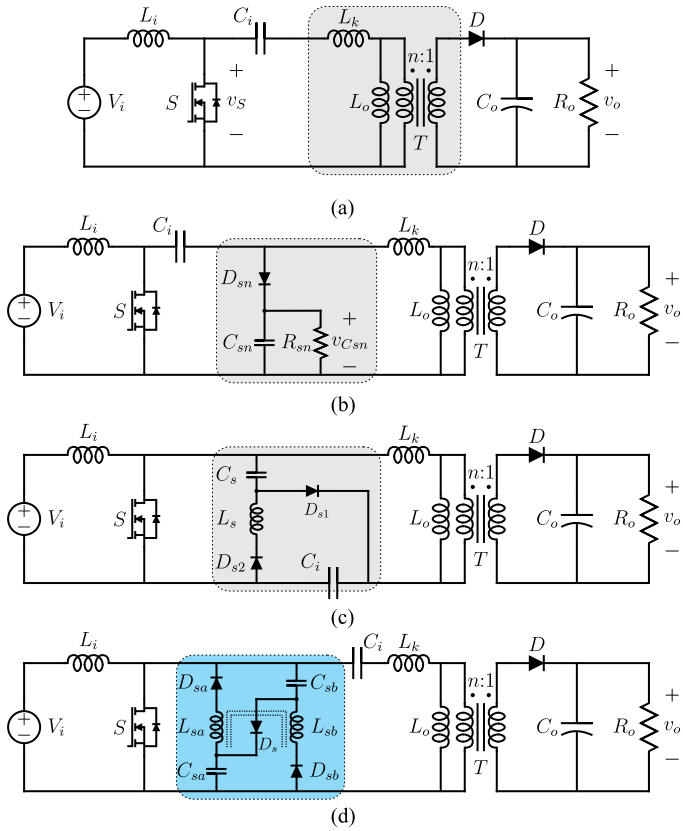

Fig. 1. (a) Isolated SEPIC converter highlighting the transformer model which includes the magnetizing and leakage inductances. (b) Isolated SEPIC using an RCD snubber cell (highlighted). (c) Modified Domb–Redl–Sokal snubber applied to the isolated SEPIC (highlighted). (d) Isolated SEPIC using the proposed regenerative snubber cell (highlighted), where the dashed line represents the optional coupling between the snubber inductors.

Manuscript received September 13, 2016; revised December 1, 2016; accepted January 9, 2017. Date of publication January 16, 2017; date of current version August 2, 2017. Recommended for publication by Associate Editor Dr. L. Huber.

G. Tibola, E. Lemmen, and J. L. Duarte are with the Department of Electrical Engineering, Eindhoven University of Technology, Eindhoven 5612 AZ, The Netherlands (e-mail: g.tibola@tue.nl; e.lemmen@tue.nl; j.l.duarte@tue.nl).

I. Barbi is with the Department of Automation and Systems, Federal University of Santa Catarina, Florianópolis 88040-900, Brazil (e-mail: ivobarbi@gmail.com).

Color versions of one or more of the figures in this paper are available online at http://ieeexplore.ieee.org.

Digital Object Identifier 10.1109/TPEL.2017.2653940

active clamp circuits [6]–[9]. The last one typically provides zero voltage switching (ZVS), but the main drawback is the addition of one or more switches; which increases cost, compromises reliability, and requires complex drivers. A more robust solution is the conventional dissipative resistor-capacitor-diode (RCD) snubber circuit, which can be placed directly across the switch or across the transformer primary side as depicted in Fig. 1(b). The RCD snubber is composed of resistor $R_{\rm sn}$, capacitor $C_{\rm sn}$, and diode $D_{\rm sn}$. This is a cost effective solution but all the energy stored in the leakage is converted to heat, reducing the converter efficiency. Besides that, if a higher isolation level is required, the leakage inductance becomes relatively high, making the use of an RCD snubber impractical due to the high dissipation.

In order to cope with high stray inductances passive regenerative snubbers for SEPIC have been proposed, such as presented in [10]–[13]. However, most of them are used in transformerless versions or their addition compromises the isolation. The SEPIC is a converter with an energy-storing transformer and for this reason energy regenerative snubber solutions as applicable for flybacks have been investigated as well [14]–[19]. Among these solutions, the most popular is the Domb–Redl–Sokal snubber [14]. In the flyback situation, the energy stored in the leakage inductance is first absorbed in the snubber capacitor and further returned to the power source through a snubber inductor. An improvement for this approach was proposed in [17] using a tertiary winding on the flyback transformer core, reducing the component count but maintaining the principle of operation. However, the SEPIC input has a current source characteristic due to the input inductor and therefore the previous solution cannot be directly applied. Although, with proper modification, the circuit can be implemented for the SEPIC converter as presented in [19]. Fig. 1(c) shows the application of this modified Domb–Redl–Sokal snubber applied to the isolated SEPIC, where the snubber inductor L_s can be coupled to the main transformer, such as in [17]. The energy stored in the leakage in this situation is first recycled to the SEPIC decoupling capacitor C_i and then transferred to the output, rather than to the input source. Extra benefits of this solution, observed by simulation in [19], are the ZVS turn-off and zero current switching turn-on.

In this perspective, this paper proposes an alternative passive regenerative snubber especially suited for isolated SEPIC converters, which combines the features of active snubbers, especially ZVS, and the robustness of passive snubber solutions. The proposed snubber cell is highlighted in Fig. 1(d) and it is composed of capacitors $C_{\rm sa}$ and $C_{\rm sb}$ ($C_{\rm sa} = C_{\rm sb} = C_s$), inductors $L_{\rm sa}$ and $L_{\rm sb}$ ($L_{\rm sa} = L_{\rm sb} = L_s$), and diodes D_s, $D_{\rm sa}$, and $D_{\rm sb}$. The introduction of this cell was first aimed at suppressing the voltage spike across the bridge leg of an isolated full-bridge boost topology [20], [21]. When applied to a SEPIC, the behavior of the snubber cell is extended with extra operational stages [22], increasing the converter efficiency when compared to the SEPIC using the RCD snubber cell [23]. Additionally, $L_{\rm sa}$ and $L_{\rm sb}$ can be coupled, as illustrated by the dashed lines in Fig. 1(d), reducing the required snubber inductance by a factor of two, and reducing the number of components in the circuit as well.

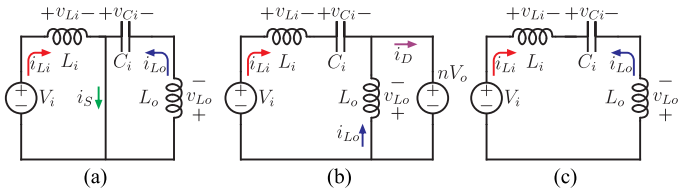

Fig. 2. SEPIC equivalent circuits for (a) first and (b) second operational stages in CCM. (c) Third operational stage valid only for DCM.

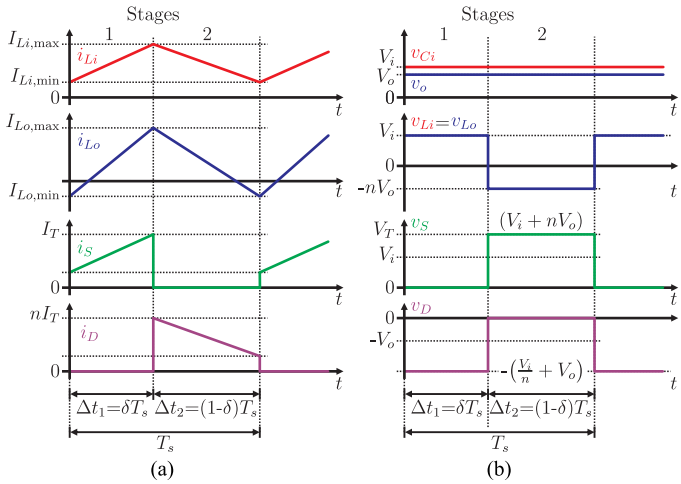

Fig. 3. (a) Main current and (b) voltage waveforms for CCM operation.

The proposed snubber has more passive components in comparison to [19] and it seems to be an extended version of that approach. However, the energy from the leakage is first stored in the snubber capacitors and then transferred to the output. This means that the decoupling capacitor is not part of the snubber circuit anymore and do not need to be fully allocated in an internal loop inside the snubber [see Fig. 1(c)]. As a consequence, C_i can still be split in two parts for symmetry, voltage stress reduction, and extra galvanic isolation purposes. Inductors $L_{\rm sa}$ and $L_{\rm sb}$ might be coupled to the main transformer, although the study to prove this assumption is not performed in this paper. However, the idea to keep the snubber circuit independent for the converter circuit is preferable in some situations. Besides that, until now, there has neither been a detailed analysis of the snubber circuit operation in [19] when applied to SEPIC available nor a complete description of practical design procedures.

The operational principle of both RCD and regenerative snubbers are analyzed in detail based on the discontinuous conduction mode (DCM) operation of the SEPIC. For continuous conduction mode (CCM), the analysis is similar and the design snubber equations obtained for DCM can be also applied by making the proper considerations with respect to the new current stress situation, as shown in this paper. Design guidelines are given for a converter specification using both snubbers. Finally, to validate the method, experimental results are shown for DCM and CCM operation using both snubbers for the sake of comparison.

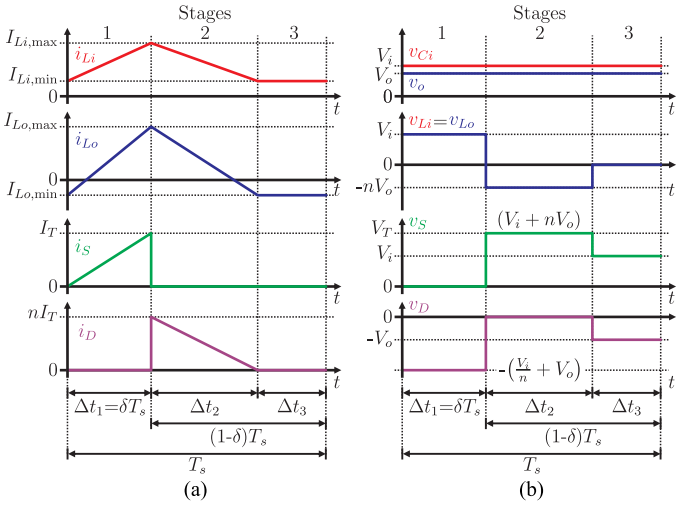

Fig. 4. (a) Main current and (b) voltage waveforms for DCM operation.

II. Review of the SEPIC

The dc–dc SEPIC can operate in CCM or DCM. The operation in CCM is detailed in [1] and this mode has two operational stages. When operating in DCM, a third stage appears as described in [2] and [24]. Fig. 2 shows three simplified equivalent circuits of the ideal SEPIC in DCM. In CCM, only the first two equivalent circuits shown in Fig. 2 exist. Figs. 3(a) and (b) and 4(a) and (b) illustrate the main current and voltage waveforms for CCM and DCM operation.

Based on the operational stages and waveforms, the time intervals that represent the duration of each stage are given by

$$\Delta t_1 = \frac{\delta}{f_s} \text{ valid for both modes} \tag{1}$$

$$\Delta t_2 = \begin{cases} \frac{(1-\delta)}{f_s} & \text{if CCM} \\ \frac{\delta V_i}{nV_o f_s} & \text{if DCM} \end{cases} \tag{2}$$

and

$$\Delta t_3 = \frac{(1-\delta)\, nV_o - \delta V_i}{nV_o f_s} \text{ valid for DCM only} \tag{3}$$

where δ is the duty-cycle and f_s is the switching frequency. For DCM operation, the peak currents in the input inductance L_i, and in the output inductance L_o are found to be

$$I_{Li,\max} = \frac{\delta V_i \left[\delta \left(nV_o L_i - V_i L_o\right) + 2nV_o L_o\right]}{2nV_o L_i L_o f_s} \tag{4}$$

and

$$I_{Lo,\max} = \frac{\delta V_i \left[2nV_o L_i - \delta \left(nV_o L_i - V_i L_o\right)\right]}{2nV_o L_i L_o f_s}. \tag{5}$$

For CCM operation, including the load current I_o, these variables are given by

$$I_{Li,\max} = \frac{V_i \delta}{2L_i f_s} + \frac{I_o \delta}{n\left(1-\delta\right)} \tag{6}$$

and

$$I_{Lo,\max} = \frac{V_i \delta}{2L_o f_s} + \frac{I_o}{n}. \tag{7}$$

For further analysis of the snubber, two important relations must be derived. The first is the maximum voltage across the switch S, that for both modes is given by

$$V_T = V_i + nV_o. \tag{8}$$

The second is the maximum current through S, which for DCM is written as

$$I_{T,\mathrm{DCM}} = I_{Li,\max} + I_{Lo,\max} = \frac{\delta V_i}{L_{eq} f_s} \tag{9}$$

whereas for CCM, it is given by

$$I_{T,\mathrm{CCM}} = I_{Li,\max} + I_{Lo,\max} = \frac{V_i \delta}{2L_{eq} f_s} + \frac{I_o}{n\left(1-\delta\right)}. \tag{10}$$

For both DCM and CCM, L_{eq} is the equivalent inductance of the converter, equal to the parallel combination of L_i and L_o, as

$$L_{\mathrm{eq}} = \frac{L_i L_o}{L_i + L_o}. \tag{11}$$

The converter gain (relation between the input voltage and output voltage V_o) is equal to

$$G = \frac{V_o}{V_i} = \begin{cases} \frac{\delta}{1-\delta} & \text{if CCM} \\ \delta\sqrt{\frac{R_o}{2L_{\mathrm{eq}} f_s}} & \text{if DCM} \end{cases} \tag{12}$$

where R_o represents the output load resistance.

When including a transformer in the circuit, the output inductance becomes equal to the magnetizing inductance. Additionally, a leakage inductance is added between the decoupling capacitor C_i and the transformer. The energy stored in this leakage causes an overvoltage across S, every time it is switched OFF. For this reason, a snubber circuit must be included. The next two sections present the analysis of the conventional RCD snubber and the proposed regenerative snubber cells applied to the isolated SEPIC. This analysis is performed for the converter operating in DCM and extended to CCM operation.

III. RCD snubber principle of operation

The addition of the RCD circuit adds an extra operational stage to the conventional DCM SEPIC, that happens after switch S is commanded to turn-off. At this moment, snubber diode D_{sn} starts conducting the current circulating in the leakage inductance L_k, transferring its energy to the snubber capacitor C_{sn}. D_{sn} also creates a path for the current circulating in L_i, which is a drawback for this snubber circuit since it discharges part of the input inductor energy. Because of this action, output diode D instead of assumes the current nI_T as in the ideal situation, its current grows following the relation:

$$i_D = n\left(i_{Lo} - i_{Lk}\right). \tag{13}$$

Considering these operation and assuming that C_{sn} is large enough, keeping voltage v_{Csn} unchanged during one switching period (T_s), the simplified equivalent circuit during this stage

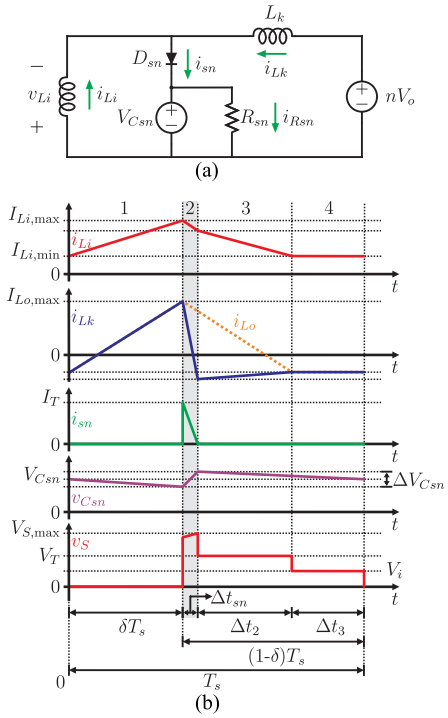

Fig. 5. (a) Equivalent circuit for the second stage when the energy stored in the leakage is transfered to the RCD snubber. (b) Key waveforms for the DCM SEPIC operating with RCD snubber highlighting the second stage.

can be drawn as illustrated in Fig. 5(a), where $C_{\rm sn}$ is replaced by the voltage source V_{Csn}. The key waveforms are depicted in Fig. 5(b), where an extra stage is added, compared to the conventional DCM SEPIC; first, third, and fourth stages have the same equivalent circuits as presented in Fig. 2(a), (b), and (c), respectively.

The duration of the second stage is much shorter than the other stages, therefore the snubber impact on the converters gain, and on the currents through the main components, can be neglected. The time of the second stage is obtained by solving the equivalent circuit and it is found to be

$$\Delta t_{\rm sn} = \frac{L_i L_k \left(I_{Li,\max} + I_{Lo,\max}\right)}{V_{Csn}\left(L_i + L_k\right) - nV_o L_i}. \tag{14}$$

The average value of the current through the snubber is equal to

$$I_{\rm sn} = \frac{\left(I_{Li,\max} + I_{Lo,\max}\right)\Delta t_{\rm sn}}{2T_s}. \tag{15}$$

Hence, the power transferred to the snubber is represented by

$$P_{\rm sn} = V_{Csn} I_{\rm sn} = \frac{V_{Csn} L_i L_k \left(I_{Li,\max} + I_{Lo,\max}\right)^2}{2T_s\left[V_{Csn}\left(L_i + L_k\right) - nV_o L_i\right]}. \tag{16}$$

As the input inductance is much larger than the leakage, (16) can be reduced and rearranged as

$$P_{\rm sn} = \frac{1}{2} L_k I_T^2 f_s \frac{1}{\left(1 - \frac{nV_o}{V_{Csn}}\right)} \tag{17}$$

where I_T is given in (9). The maximum power dissipated in the snubber is therefore larger when a smaller V_{Csn} is selected, which means that more energy than that stored in L_k is dissipated. The value of the snubber capacitor voltage V_{Csn} determines the maximum voltage across S according to

$$V_{S,\max} = V_i + V_{Csn}. \tag{18}$$

When all the energy in L_k is transferred to the snubber and $i_{Lk} = i_{Li}$, the snubber diode blocks and the output diode assumes the maximum current, starting the third stage. The energy transferred to the snubber is dissipated in the snubber resistor $R_{\rm sn}$ during the next three stages.

A. RCD Snubber Design Guidelines for DCM and CCM

The voltage ripple across the snubber capacitor can be represented by

$$\Delta V_{Csn} = \frac{I_T \Delta t_{\rm sn}}{2C_{\rm sn}}. \tag{19}$$

Then, by applying (14) and (18) in (19), and assuming $L_i \gg L_k$, an expression to obtain the value of $C_{\rm sn}$ can be derived as

$$C_{\rm sn} = \frac{L_k I_T^2}{2\Delta V_{Csn}\left(V_{S,\max} - V_T\right)} \tag{20}$$

where V_T is equal to (8). After the maximum voltage allowed across S ($V_{S,\max}$) is defined by the designer, $C_{\rm sn}$ is calculated using a value for ΔV_{Csn} between 5% and 10% of the required V_{Csn}. This is reasonable to keep the assumption that V_{Csn} is constant during the switching period. Hence, the snubber resistor is calculated by using

$$R_{\rm sn} = \frac{V_{Csn}^2}{P_{\rm sn}} = \frac{2V_{Csn}\left(V_{Csn} - nV_o\right)}{L_k f_s I_T^2}. \tag{21}$$

This resistor should be chosen with sufficient power rating based on the power loss, (17), and the required value of V_{Csn} given by $V_{Csn} = V_{S,\max} - V_i$.

For CCM operation, the presented criteria remains the same but the current I_T in (20) and (21) is replaced by the CCM relation as given in (10).

IV. Proposed Snubber Principle of Operation

When the proposed snubber circuit is added to the DCM SEPIC, as illustrated in Fig. 1(c), seven stages can be identified as depicted in Fig. 6. The key waveforms, used to analyze the principle of operation, are shown in Fig. 7. For the analysis, it is assumed that capacitors C_i and C_o are large enough to neglect the voltage ripple across them. The values of the passive components in each leg of the snubber cell are equal. However, in practice deviations can exist, which causes small changes in the waveforms but do not compromise the principle of operation. The snubber inductors are not coupled for the analysis.

A. First Stage $(t_0 < t \leq t_1)$

The operation starts when S is commanded to turn ON. The voltage across C_i is constant and equal to the input voltage V_i charging both the magnetizing inductance L_o and leakage inductance L_k. The input inductor L_i is charged through S. The voltages across $C_{\rm sa}$ and $C_{\rm sb}$ are positive, making diodes $D_{\rm sa}$

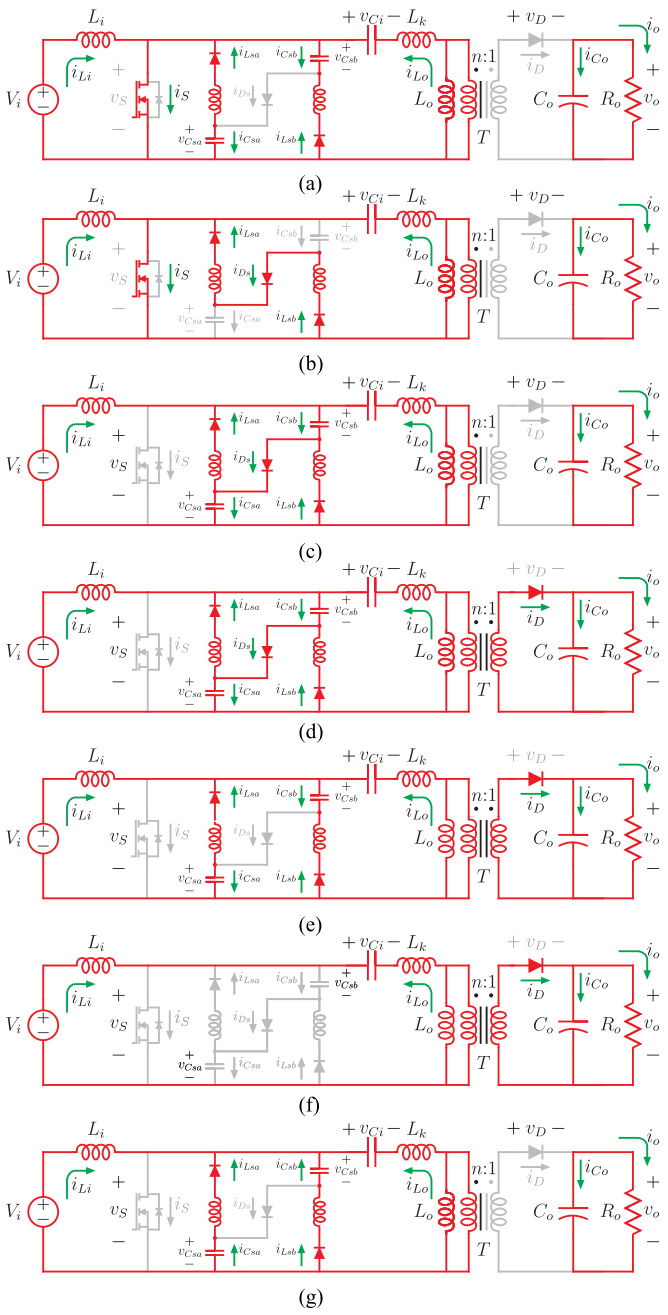

Fig. 6. Equivalent circuits per stage for the DCM SEPIC after including the proposed regenerative snubber cell. (a) First, (b) second, (c) third, (d) fourth, (e) fifth, (f) sixth, and (g) seventh stages.

and $D_{\rm sb}$ conduct, charging inductors $L_{\rm sa}$ and $L_{\rm sb}$. The output diode D is blocked and the load is maintained by the output capacitor C_o. The current paths are illustrated in Fig. 6(a). The time interval during this stage is given by

$$t_{01} = \sqrt{L_s C_s}\left[\frac{\pi}{2} - \arcsin\left(\frac{I_{Ls0}}{\sqrt{\frac{C_s}{L_s}V_{Cs0}^2 + I_{Ls0}^2}}\right)\right] \tag{22}$$

with V_{Cs0} and I_{Ls0} representing the initial values of the voltage across the snubber capacitor and current through the snubber inductor.

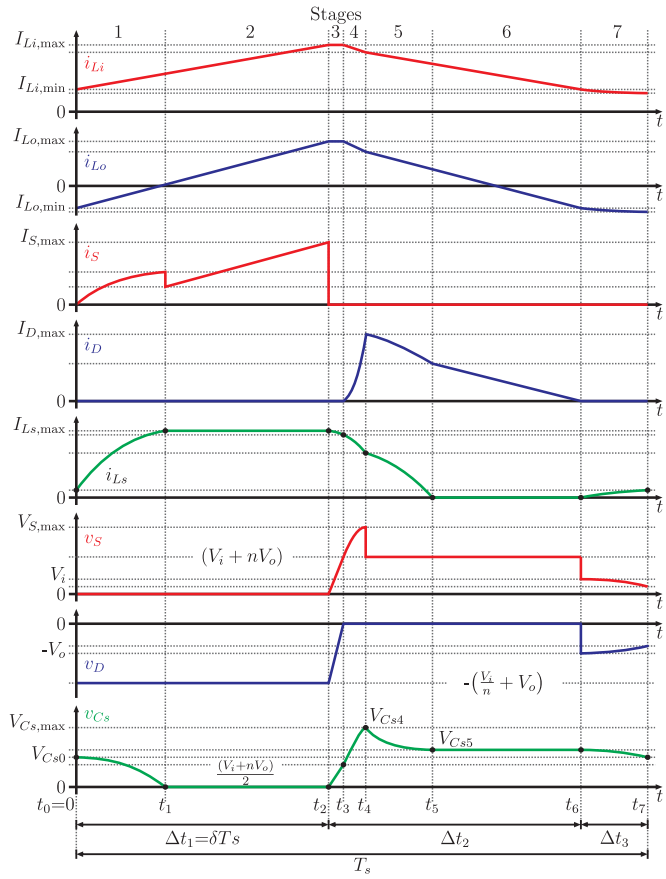

Fig. 7. Ideal waveforms to show the proposed snubber principle of operation.

The voltage across $C_{\rm sa} = C_{\rm sb} = C_s$ during this time is represented by

$$v_{Cs01}(t) = V_{Cs0}\cos(\omega_1 t) - I_{Ls0}\sin(\omega_1 t) \tag{23}$$

while the current through $L_{\rm sa} = L_{\rm sb} = L_s$ is found to be

$$i_{Ls01}(t) = \frac{V_{Cs0}}{Z_1}\sin(\omega_1 t) + I_{Ls0}\cos(\omega_1 t) \tag{24}$$

where the resonance frequency ω_1 and impedance Z_1 are calculated by

$$\omega_1 = \frac{1}{\sqrt{L_s C_s}} \tag{25}$$

and

$$Z_1 = \sqrt{\frac{L_s}{C_s}}. \tag{26}$$

At the end of the stage, all the energy stored in C_s is transferred to L_s, making the values of v_{Cs} and i_{Ls} in $t = t_{01}$ equal to

$$V_{Cs1} = v_{Cs01}(t_{01}) = 0 \tag{27}$$

and

$$I_{Ls1} = \frac{\sqrt{V_{Cs0}^2 + (Z_1 I_{Ls0})^2}}{Z_1} = I_{Ls,\max}. \tag{28}$$

B. Second Stage $(t_1 < t \leq t_2)$

When all the energy stored in the snubber capacitors is transferred to the snubber inductors, the diode D_s starts conduct, keeping the currents i_{Lsa} and i_{Lsb} ($i_{Lsa} = i_{Lsb}$) in freewheeling through the switch, as Fig. 6(b) shows. The time duration in the second stage is

$$t_{12} = \Delta t_1 - t_{01} \tag{29}$$

where Δt_1 is the same time for the ideal converter as in (1). The final values of v_{Cs} and i_{Ls} in $t = t_{12}$ are

$$V_{Cs2} = V_{Cs1} = 0 \tag{30}$$

and

$$I_{Ls2} = I_{Ls1} = I_{Ls,\max}. \tag{31}$$

C. Third Stage $(t_2 < t \leq t_3)$

In the end of the second stage, S is switched OFF, starting the third stage. As the current through the leakage inductance can not change instantaneously, it charges $C_{\rm sa}$ and $C_{\rm sb}$ through D_s. This also creates a path for the currents through L_i, $L_{\rm sa}$, and $L_{\rm sb}$. The voltages across the snubber capacitors start to grow while the voltage across the output diode (v_D) decreases. Fig. 6(c) represents the equivalent circuit for this stage. The time stage duration is

$$t_{23} = \frac{C_s V_T}{2\left(I_T + I_{Ls,\max}\right)} \tag{32}$$

where the voltage V_T and current I_T are calculated using expressions (8) and (9). As I_T can be considered constant, the voltage across C_s grows linearly in a short time and can be expressed by

$$v_{Cs23}(t) = \frac{\left(I_T + I_{Ls,\max}\right)}{C_s} t. \tag{33}$$

In the same way, current through L_s is given as

$$i_{Ls23}(t) = I_{Ls,\max} - \frac{V_T}{4L_s} t. \tag{34}$$

In $t = t_{23}$, the final values of v_{Cs} and I_{Ls} are found to be

$$V_{Cs3} = \frac{V_T}{2} \tag{35}$$

and

$$I_{Ls3} = I_{Ls,\max} - \frac{C_s V_T^2}{8L_s\left(I_T + I_{Ls,\max}\right)}. \tag{36}$$

D. Fourth Stage $(t_3 < t \leq t_4)$

In the moment v_{Cs} reaches $V_T/2$, v_D becomes equal to zero and D starts to conduct, initiating the fourth stage. During this stage, Fig. 6(d), the voltage across C_s continues to rise until all the energy stored in L_k is transferred, blocking D_s and starting the next stage. The time interval is defined as

$$t_{34} = \frac{\pi}{2}\sqrt{\frac{L_k C_s}{2}}. \tag{37}$$

The evolution of v_{Cs} and i_{Ls} is represented by

$$v_{Cs34}(t) = V_{Cs3} + Z_2\left(I_T + I_{Ls3}\right)\sin\left(\omega_2 t\right) \tag{38}$$

and

$$i_{Ls34}(t) = I_{Ls3} - \frac{1}{L_s}\int_0^t v_{Cs34}(t)\,dt \tag{39}$$

where the resonance frequency ω_2 and impedance Z_2 are calculated by

$$\omega_2 = \sqrt{\frac{2}{L_k C_s}} \tag{40}$$

and

$$Z_2 = \sqrt{\frac{L_k}{2C_s}}. \tag{41}$$

Applying (37) in (38) and (39), the voltage value across C_s and current through L_s in $t = t_{34}$ become

$$V_{Cs4} = \frac{V_T}{2} + Z_2\left(I_T + I_{Ls3}\right) \tag{42}$$

and

$$I_{Ls4} = I_{Ls3} - \left[\frac{V_T \pi\sqrt{2L_k C_s} + 4L_k\left(I_T + I_{Ls3}\right)}{8L_s}\right]. \tag{43}$$

The sum of v_{Csa} and v_{Csb}, or twice V_{Cs4}, defines the maximum voltage stress across the switch S

$$V_{S,\max} = 2V_{Cs4} = V_T + 2Z_2\left(I_T + I_{Ls3}\right). \tag{44}$$

E. Fifth Stage $(t_4 < t \leq t_5)$

When all the energy stored in L_k is transferred to the snubber D_s blocks starting the fifth stage, which is illustrated by the circuit depicted in Fig. 6(e). The output diode assumes the current in L_i and L_o, plus the current of $L_{\rm sa}$ and $L_{\rm sb}$, respecting the transformer relation as

$$I_{D,\max} = n\left(I_T + 2I_{Ls4}\right). \tag{45}$$

As $D_{\rm sa}$ and $D_{\rm sb}$ are conducting, v_S drops instantaneously to V_T, while C_s discharges during the time interval

$$t_{45} = \frac{\theta}{\omega_1} \tag{46}$$

where $0 < \theta < \pi$ is given by

$$\theta = \arctan\left(\frac{Z_1 I_{Ls4}}{V_T - V_{Cs4}}\right). \tag{47}$$

During any time in this interval, the voltage across C_s is represented by

$$v_{Cs45}(t) = V_T - \left(V_T - V_{Cs4}\right)\cos\left(\omega_1 t\right) - Z_1 I_{Ls4}\sin\left(\omega_1 t\right) \tag{48}$$

while the current through L_s is

$$i_{Ls45}(t) = \frac{V_T}{Z_1}\sin\left(\omega_1 t\right) - I_{Ls4}\cos\left(\omega_1 t\right). \tag{49}$$

In the end of the fifth period, all the energy from the leakage inductance, temporally stored in the snubber circuit, is transferred to the output. The remaining energy in L_s is transferred to C_s (tank circuit). Then, $V_{Cs5} = v_{cs}(t_{45})$ and $I_{Ls5} = 0$.

F. Sixth Stage ($t_5 < t \leq t_6$)

As $i_{Lsa} = i_{Lsb} = 0$, $D_{\rm sa}$ and $D_{\rm sb}$ block while C_s remains charged with the voltage V_{Cs5}, starting the sixth stage. As seen in Fig. 6(f), the snubber is not conducting in this interval. In this stage, the normal SEPIC operation remains until all the energy stored in the input and magnetizing inductances is transferred to the output. The time interval is then represented by

$$t_{56} = \Delta_{t2} - (t_{23} + t_{34} + t_{45}) \tag{50}$$

where Δt_2 is calculated using (2). The final values of the snubber capacitor voltages and snubber inductor currents are $V_{Cs6} = V_{Cs5}$ and $I_{Ls6} = I_{Ls5} = 0$.

G. Seventh Stage ($t_6 < t \leq t_7$)

The last stage starts when the current in the magnetizing inductance i_{Lo} becomes equal, in modulus, to the input current i_{Li}, blocking the output diode. This is the discontinuous period where all power semiconductors are blocked. The load is supplied by C_o and a constant current flows in the primary-side circuit. As the voltage across the snubber capacitors is larger than the voltage across S, diodes $D_{\rm sa}$ and $D_{\rm sb}$ are forward biased. The current through the inductor snubber starts to grow, decreasing the voltage across C_s and consequently V_S decreases as well. The minimum current that circulates through L_i and L_o, which is normally constant, slightly decreases according to i_{Ls}. Fig. 6(g) shows the last equivalent circuit which remains active until S is turned ON again, restarting the cycle. The time duration t_{67} is equal to Δt_3, as in (3).

The voltage across C_s and the current through L_s during this interval are given by

$$v_{Cs67}(t) = V_i - (V_i - V_{Cs6})\cos(\omega_3 t) \tag{51}$$

and

$$i_{Ls67}(t) = \frac{V_{Cs6} - V_i}{Z_3}\sin(\omega_3 t) \tag{52}$$

where the resonance frequency ω_3 and impedance Z_3 are

$$\omega_3 = \frac{1}{\sqrt{L_{\rm eq2} C_s}} \tag{53}$$

and

$$Z_3 = \sqrt{\frac{L_{\rm eq2}}{C_s}}. \tag{54}$$

The parameter $L_{\rm eq2}$ represents the equivalent inductance of the series combination of L_s, L_o, and L_k as

$$L_{\rm eq2} = L_s + 2(L_o + L_k). \tag{55}$$

After the interval t_{67}, the final value of v_{Cs} and i_{Ls} are

$$V_{Cs7} = v_{Cs67}(\Delta t_3) = V_{Cs0} \tag{56}$$

and

$$I_{Ls7} = i_{Ls67}(\Delta t_3) = I_{Ls0}. \tag{57}$$

The peculiarity of this stage is that for maximum power transfer (worst scenario) Δt_3 is too short, making the variations of v_{Cs} and i_{Ls} too small that can be neglected. This fact makes

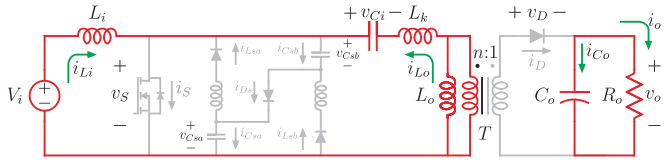

Fig. 8. Eighth equivalent circuit.

$V_{Cs7} = V_{Cs5}$ and $I_{Ls7} = 0$. In the other hand, for small power processing, when t_{67} is larger than π/ω_3, the current in L_s completes half-cycle of the resonance period. As $D_{\rm sa}$ and $D_{\rm sb}$ do not conduct negative currents, the final value of i_{Ls}, in this situation, is zero, while v_{Cs7} is calculated by

$$V_{Cs7} = 2V_i - V_{Cs5} = V_{Cs0}. \tag{58}$$

The final values of v_S, i_{Li}, and i_{Lo} in this condition return to the initial values in the stage that are

$$V_{S7} = V_{S6} = V_i \tag{59}$$

and

$$I_{Li,\min} = -I_{Lo,\min} = \frac{\delta^2 V_i\,(nV_oL_i - L_oV_i)}{2nV_o f_s L_i L_o}. \tag{60}$$

If this situation occurs, an eighth stage starts where the snubber circuit is not conducting, as represented by the equivalent circuit shown in Fig. 8.

V. Regenerative Snubber Design Criteria

The equations presented in the previous section describe the snubber principle of operation. A straight way to design its components is by following sequential steps in a recursive cycle. However, this is an impractical process and simplified equations are always useful, even if the outcomes provide only approximations. In this perspective, two extra equations would be helpful. The first one should estimate the minimum value of the snubber capacitor for a desired peak switch voltage and the second giving the snubber inductor values in order to satisfy the operational principle and to minimize the losses caused by the snubber addition.

A. Snubber Capacitor Value

The maximum voltage across S is defined by (44). For larger values of C_s, the value of I_{Ls3} in (36) and the second term in (44) become smaller, reducing the voltage stress in S. Therefore, the maximum voltage across S can be simplified as

$$V_{S,\max} = V_T + 2Z_2 I_T. \tag{61}$$

Substituting (41) in (61) gives an approximate expression to calculate C_s for a desired $V_{S,\max}$ as

$$C_s = \frac{2L_k I_T^2}{(V_{S,\max} - V_T)^2}. \tag{62}$$

The maximum voltage is determined by the designer and must be larger than V_T and smaller than the maximum voltage allowed for the chosen semiconductor. The ideal snubber capacitor could be selected for $V_{S,\max} = V_T$, although the result would be a

large C_s value. Doing so, it increases the time intervals to transfer the energy stored in the leakage to C_s and later to the output. This time has a direct influence in the converter characteristics, and, in order not to affect the gain, it must remain as short as possible. Then, it is recommended to keep the clamp voltage as high as possible or make adjustments in the converter design, taking into account the gain loss caused by the snubber presence.

B. Snubber Inductor Value

Considering the maximum power transfer, the current through L_s in the beginning of the first stage is approximately zero. The voltage V_{Cs0} is equal to V_{Cs5}, and for simplification, can be approximated by $V_T/2$. Then, the maximum current $I_{Ls,\max}$ can be written as

$$I_{Ls,\max} \approx \frac{V_T}{2Z_1}. \tag{63}$$

To match the assumption made in (62), that $I_{Ls,\max}$ is neglected, this current must be significantly smaller than I_T. Then, taking this aspect into account and substituting (26) in (63), a minimum value for L_s is calculated as

$$L_{s,\min} > \frac{C_s V_T^2}{4k^2 I_T^2} \tag{64}$$

where k represents the percentage of I_T and it is recommended to be between 10% and 20% ($0.1 < k \leq 0.2$).

Now, once the minimum value is defined, the designer has the freedom to choose a value for L_s. The value of L_s has a direct impact on the conduction losses as it increases the current through the semiconductors. Although after a certain value, the effect is not relevant anymore. A maximum value is calculated in order to keep the principle of operation unchanged. Again, by analyzing the first stage, it can be noticed that the maximum value of L_s should be chosen such that the time t_{01} is smaller than Δt_1. Using the previous assumption that $I_{Ls0} = 0$, t_{01} is written as

$$t_{01} = \frac{\pi}{2}\sqrt{L_s C_s}. \tag{65}$$

Hence, the upper limit for L_s is found to be

$$L_{s,\max} < \frac{4\delta^2}{C_s \pi^2 f_s^2}. \tag{66}$$

C. CCM Consideration

The analysis in DCM using the regenerative snubber uses the parameter I_T for DCM (9). The main difference when operating in CCM is the absence of the seventh stage, since $\Delta_{t3} = 0$. Hence, knowing that the design criteria for DCM already neglects the seventh stage, though the same expressions for DCM can be used to define the snubber for CCM operation. The only necessary modification is to change current I_T in (62) and (64) for the CCM current relation given by (10).

D. Considerations on Losses

Despite the fact that the proposed snubber recovers the energy stored in the leakage inductance, its addition to the circuit causes an increment in the conduction losses when compared to the converter without snubber. Besides, losses in the snubber components, mainly in the inductors, must also be taken into account. For this reason, a good design and component choice is necessary. Contrary to the RCD losses calculation, the complete losses analyses for the regenerative snubber is too cumbersome since the expressions to calculate the rms values of the currents through the components must be derived and this goes over the scope of this paper, although this process can be done by simulation in order to estimate the losses if necessary. However, the impact of losses is essentially caused by the snubber inductor choice. For instance, if L_s is dimensioned to have a value close to the limit, (66), the rms value of the currents through S and D become close to the ideal values, minimizing the conduction losses. In Fig. 9, this example is graphically proved by comparing the commutation current

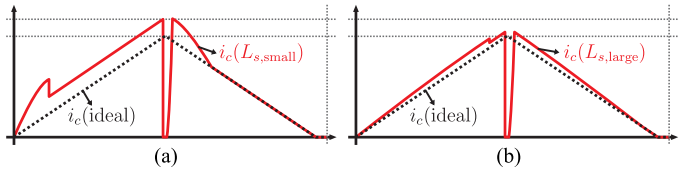

Fig. 9. Commutation currents for (a) small and (b) large values of L_s, both compared to the ideal commutation current represented by the dashed lines.

$$i_c = i_S + \frac{i_D}{n} \tag{67}$$

with the idealized commutation current for two different values of L_s. It is clear that for a large value of L_s, Fig. 9(b), the rms value of the commutation current is close to the ideal one, reducing the conduction losses, although a compromise between losses and the volume of L_s is necessary. Nevertheless, with a good design, an improvement in efficiency is expected when using the regenerative snubber instead of the RCD one.

Commutation losses are not analyzed into details in this study, although the proposed snubber helps to reduce these losses since it provides ZVS, such as the solution in [19].

VI. Experimental Results

In order to validate the proposed snubber concept, a converter prototype was built as shown in Fig. 10(a). The converter was first designed to operate in DCM. Later the operation for CCM was achieved by replacing the input and magnetizing inductors. The regenerative snubber cell is highlighted in Fig. 10(a) and it can be replaced by the RCD snubber cell shown in Fig. 10(b) or by the regenerative snubber with coupled inductors depicted in Fig. 10(c). Table I shows the converter specifications while Table II summarizes the main design parameters for both DCM and CCM. For the switch S, a 600 V MOSFET has been used and the maximum voltage to design the snubber components was specified in $V_{S,\max} = 400$ V. Components' part number are shown in Table III.

Both snubbers (regenerative and RCD) in DCM and CCM were designed according to the guidelines, specification, and obtained converter parameters. The calculated duty cycle for nominal power is $\delta = 0.477$ for DCM and $\delta = 0.5$ for CCM.

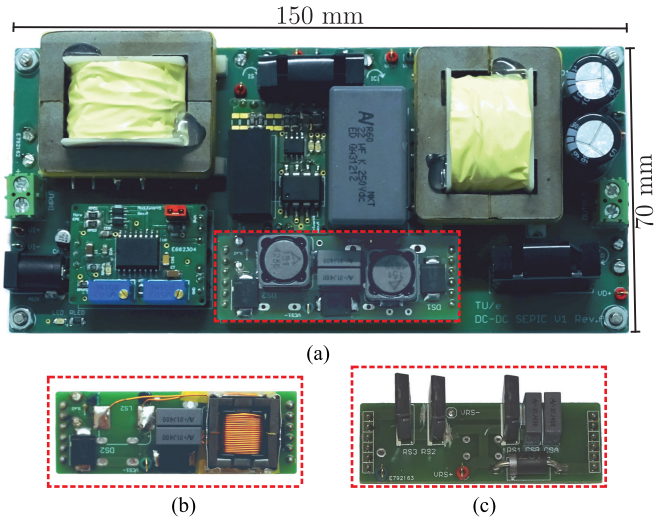

Fig. 10. (a) 100 W experimental prototype including the proposed regenerative snubber cell (highlighted). (b) Regenerative snubber cell using coupled inductors. (c) RCD snubber cell.

TABLE I
GENERAL SPECIFICATIONS

Specification	Value
Rated power (P_o)	100 W
Input voltage (V_i)	100 V
Output voltage (V_o)	50 V
Switching frequency (f_s)	50 kHz

TABLE II
DESIGNED PARAMETERS

Converter Parameters	DCM	CCM
Decoupling capacitor (C_i)	22 μF	22 μF
Output capacitor (C_o)	1120 μF	1120 μF
Input inductance (L_i)	3.84 mH	3.09 mH
Magnetizing inductance (L_o)	211.7 μH	1.43 mH
Transformer turns ratio (n)	2	2
Leakage inductance (L_k)	8.7 μH	32.55 μH
Regenerative Snubber Parameters	**DCM**	**CCM**
Snubber capacitors ($C_{\rm sa}$ and $C_{\rm sb}$)	10 nF	10 nF
Snubber inductors ($L_{\rm sa}$ and $L_{\rm sb}$)	220 μH	1 mH
RCD Snubber Parameters	**DCM**	**CCM**
Snubber capacitor ($C_{\rm sn}$)	20 nF	20 nF
Snubber resistor ($R_{\rm sn}$)	10 kΩ	10 kΩ

The snubbers designed parameters are provided in Table II as well. The experimental results summarized in this section were obtained in open loop for both operational modes and snubber options.

A. DCM Operation With Proposed Regenerative Snubber

The first experimental result, which validates the operational modes and proposed regenerative snubber principle of operation, is presented in Fig. 11. It shows the voltage across the switch S, the currents through S, and the output diode D. It is possible to see the moments where the energy from the leakage

TABLE III
MAIN COMPONENTS PART NUMBER

Power Components	Part Number
Switch (S)	IPP60R160C6
Diode (D)	MUR820G
Decoupling capacitor (C_i)	R60IR52205000K
Output capacitor (C_o)	EEUFR1J561L
Transformer cores (T) (DCM/CCM)	E42/17/12-3C92
Inductor cores (L_i) (DCM/CCM)	E42/17/12-3C92
Regenerative Snubber Components	**Part Number**
Snubber capacitors ($C_{\rm sa}$ and $C_{\rm sb}$)	R76MD2100SE40J
Snubber inductors (DCM) ($L_{\rm sa}$ and $L_{\rm sb}$)	B82477P4224M000
Snubber inductors (CCM) ($L_{\rm sa}$ and $L_{\rm sb}$)	MSS1246T-105KL_
Snubber coupled inductor core (L_s)	B66413G0000X187
Snubber diodes ($D_{\rm sa}$, $D_{\rm sb}$ and D_s)	ES3G-E3/57T
RCD Snubber Components	**Part Number**
Snubber capacitor ($C_{\rm sn}$)	R76MD2100SE40J
Snubber diode ($D_{\rm sn}$)	MUR460
Snubber resistor ($R_{\rm sn}$)	MP925-20.0K-1%

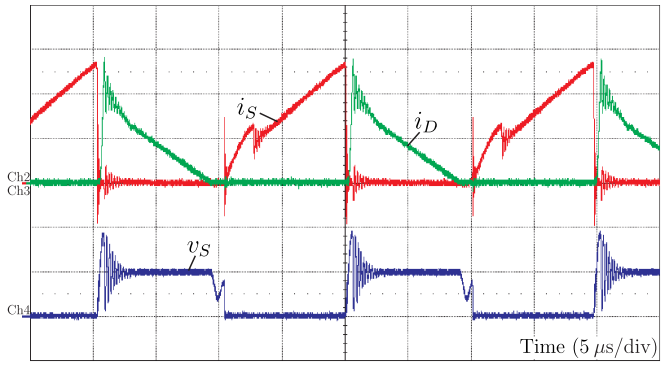

Fig. 11. Experimental results in DCM for nominal power with regenerative snubber: Current (2 A/div) through and voltage (200 V/div) across the switch S and current (5 A/div) through the output diode D.

inductance is temporarily stored in the snubber and posteriorly transferred to the output. This confirms the goal of the proposed snubber cell.

Fig. 12(a) again depicts the voltage across the switch S together with the current through it, but on a different time scale. The maximum value of the voltage v_S agrees with the theoretical expectation (≈400 V). The small difference between the theoretical and experimental values is due to the practical implementation of the components. The theoretical value of C_s, according to (62), would be equal to approximately 8.7 nF, although a commercial value of 10 nF capacitor has been selected. Hence, rearranging (62), the expected maximum voltage across S is recalculated by

$$V_{S,\max} = V_T + I_T\sqrt{\frac{2L_k}{C_s}}. \tag{68}$$

Fig. 12(b) presents a close-up view of the switch turn-off process, where it is possible to visualize the ZVS feature, while Fig. 12(c) shows the current and voltage in the output diode. The current through L_i, same as the input current, together with the current through the transformer primary side is depicted

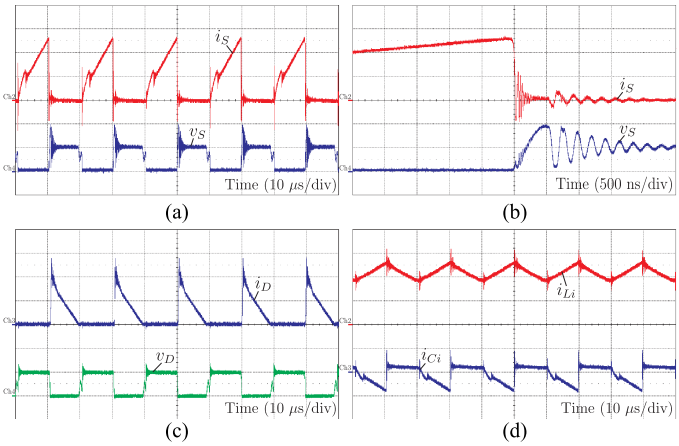

Fig. 12. Experimental results in DCM for nominal power with regenerative snubber: (a) Current (2 A/div) through and voltage (200 V/div) across the switch S. (b) Turn-off detail of the current (2 A/div) through and voltage (200 V/div) across the switch S. (c) Current through (5 A/div) and reverse voltage (100 V/div) across the output diode D. (d) Current through the input inductor (500 mA/div) and current through the capacitor C_i (transformer primary side) (5 A/div).

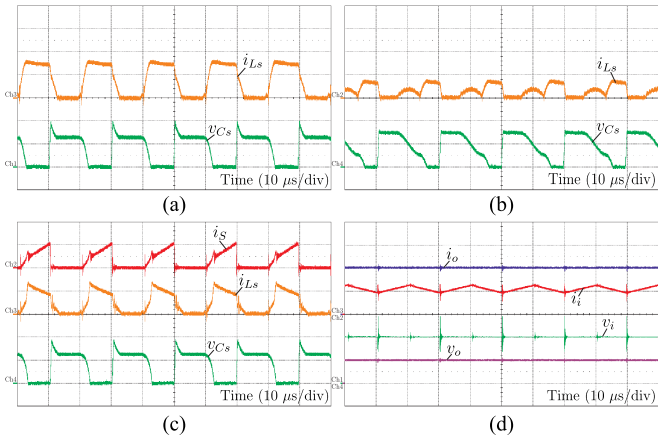

Fig. 13. Experimental results in DCM with regenerative snubber: Current through one snubber inductor (500 mA/div) and voltage across one snubber capacitor (100 V/div) for (a) nominal load and (b) light load. (c) Current through S (5 A/div), current through one snubber inductor (1 A/div), and voltage across one snubber capacitor (100 V/div) when using the snubber inductors coupled. (d) Input and output currents (1 A/div) together with input and output voltages (50 V/div) for nominal power.

in Fig. 12(d). The peaks are in agreement with the analytical maximum values.

The current through the snubber inductor together with the voltage across the snubber capacitor can be found in Fig. 13(a). The results are in agreement with the principle of operation and match the simulated values presented in [22]. As mentioned, for light loads, the seventh stage is more evident since the discontinuous time of the converter is larger. The eighth stage occurs after the current through L_s completes a half-cycle of the resonant tank circuit. This expected behavior is spotted in the experimental result presented in Fig. 13(b), which again shows the current through the snubber inductor together with the voltage across the snubber capacitor, but for light load.

One advantage of the proposed snubber is the possibility, due to the symmetry, to couple the snubber inductors. By doing so,

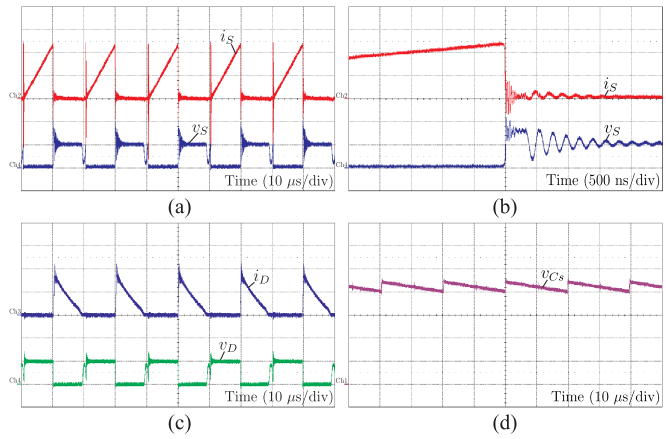

Fig. 14. Experimental results in DCM for nominal power with RCD snubber: (a) Current (2 A/div) through and voltage (200 V/div) across the switch S. (b) Turn-off detail of the current (2 A/div) through and voltage (200 V/div) across the switch S. (c) Current through (5 A/div) and reverse voltage (100 V/div) across the output diode D. (d) Voltage across the snubber capacitor (50 V/div).

the equivalent snubber inductance is found to be

$$L_{s,\text{coupled}} = \frac{L_s}{2}. \tag{69}$$

Within this possibility, the number of components is reduced, however the necessary magnetic volume and snubber losses remain the same. Fig. 13(c) shows the current through S, the current through one of the coupled snubber inductors together with the voltage across the snubber capacitor. In this situation, the coupled inductance value is equal to 160 μH. As can be visualized in the current, the transition from the first to the second stage is slightly different from the theory due to the coupling nonidealities. Nevertheless, the result is still in agreement, and validates the possibility to use coupled inductors.

The input and output voltages and currents are presented in Fig. 13(d) in order to demonstrate the expected operation of the DCM SEPIC converter and maximum power transfer.

B. DCM Operation With RCD Snubber

Fig. 14 presents a set of experimental results using the RCD snubber. In Fig. 14(a), it is possible to see the voltage across the switch S together with the current through it. The maximum value of the voltage v_S agrees with the theoretical value (≈400 V). A detailed view of the switch turn-off process is depicted in Fig. 14(b). Fig. 14(c) shows the current and voltage in the output diode while the voltage across the snubber capacitor can be seen in Fig. 14(d). The results are in accordance with the principle of operation, although small differences in the switch maximum voltage and snubber capacitor voltage values are present. These deviations are due to the simplifications made in the analysis and also because the commercial values of the components are different from the calculated ones.

In order to find the exact values or make the results to be closer to the specifications, the voltage V_{Csn} must be recalculated after choosing R_{sn} by

$$V_{Csn} = \frac{nV_o}{2} + \frac{1}{2}\sqrt{2R_{\text{sn}}L_k f_s I_T^2 + n^2 V_o^2}. \tag{70}$$

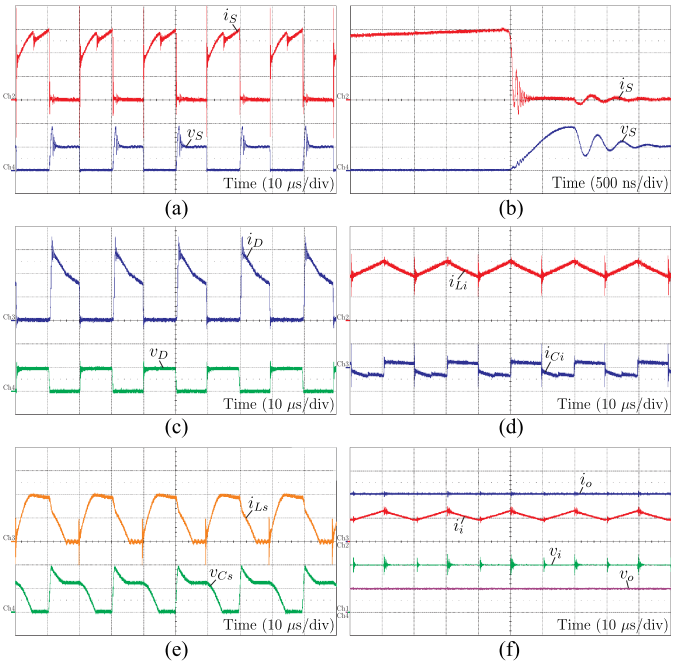

Fig. 15. Experimental results in CCM for nominal power with regenerative snubber: (a) Current (1 A/div) through and voltage (200 V/div) across the switch S. (b) Turn-off detail of the current (1 A/div) through and voltage (200 V/div) across the switch S. (c) Current through (2 A/div) and reverse voltage (100 V/div) across the output diode D. (d) Current through the input inductor (500 mA/div) and current through the capacitor C_i (transformer primary side) (5 A/div). (e) Current through one snubber inductor (200 mA/div) and voltage across one snubber capacitor (100 V/div). (f) Input and output currents (1 A/div) together with input and output voltages (50 V/div).

With the new value of V_{Csn}, the actual dissipated power is calculated using (17) while the ΔV_{Csn} using the chosen $C_{\rm sn}$ is reobtained with (19). Then, the maximum voltage across S is given by

$$V_{S,\max} = V_i + V_{Csn} + \frac{\Delta V_{Csn}}{2}. \tag{71}$$

C. CCM operation With Proposed Regenerative Snubber

When the SEPIC is operating in CCM using the regenerative snubber, the seventh stage does not exist. However, the derived equations used for DCM to design the snubber components remain the same. The difference is the current I_T, that is calculated using (10) for CCM. Fig. 15 summarizes the main experimental results for the CCM SEPIC with regenerative snubber. In Fig. 15(a), switch voltage and current are presented with a turn-off detail shown in Fig. 15(b). The output diode voltage and current are shown in Fig. 15(c). In this result, it is noticeable that the snubber action and the conclusion are the same as for DCM. Fig. 15(d) presents the input inductor current and current through the transformer primary side, while Fig. 15(e) shows the current through one snubber inductor and voltage across on snubber capacitor. For the sake of comparison with the DCM operation, Fig. 15(f) depicts the input and output voltages and currents. The results for CCM are also in agreement with the theory and the voltage across the switch is clamped to the specified value (around 400 V), while the energy stored in the transformer leakage inductance is transferred to the output.

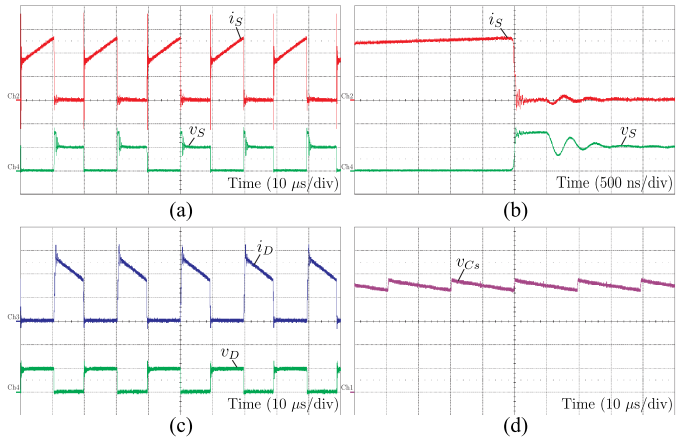

Fig. 16. Experimental results in CCM for nominal power with RCD snubber: (a) Current (1 A/div) through and voltage (200 V/div) across the switch S. (b) Turn-off detail of the current (1 A/div) through and voltage (200 V/div) across the switch S. (c) Current through (2 A/div) and reverse voltage (100 V/div) across the output diode D. (d) Voltage across the snubber capacitor (50 V/div).

D. CCM Operation With RCD Snubber

As for DCM, the converter operating in CCM was tested using the RCD snubber in order to compare the results with the regenerative cell. The main waveforms are presented in Fig. 16. The snubber design for CCM is the same as for DCM but, once again, applying the CCM corresponding I_T current from (10). The voltage across S is clamped around the same value as with the regenerative snubber, as can be noticed in Fig. 16(a), with details in Fig. 16(b). Fig. 16(c) presents the output diode current and voltage, while Fig. 16(d) shows and snubber capacitor voltage. The same conclusions as for DCM can drawn for the CCM operation.

E. Efficiency Comparison

The efficiency curves (η versus P_o) for different loads and conditions are given in the plot depicted in Fig. 17. Fig. 17(a) shows the comparison of the converter efficiency in DCM between an RCD and the proposed regenerative snubber. The values are satisfactory to validate the use of the proposed snubber and an improvement around 3% in efficiency is obtained using the regenerative cell. For low loads, the efficiency improvement is about 5%.

In Fig. 17(b), the converter efficiency in DCM using the regenerative snubber is present for two different snubber inductor values (220 and 470 μH), and for a coupled inductor. It is clear that for larger values of L_s, the efficiency is improved since the rms value of the currents through S and D reduces, as expected (see Fig. 9). By using the coupled inductor, the efficiency is slightly better when compared to $L_s = 220\,\mu H$. But as in this case the coupled inductor $L_{s,\rm coupled} = 160\,\mu H$, it could only be compared with separated inductors of $L_s = 320\,\mu H$. However, the main advantage for coupling is the reduction of the magnetic parts.

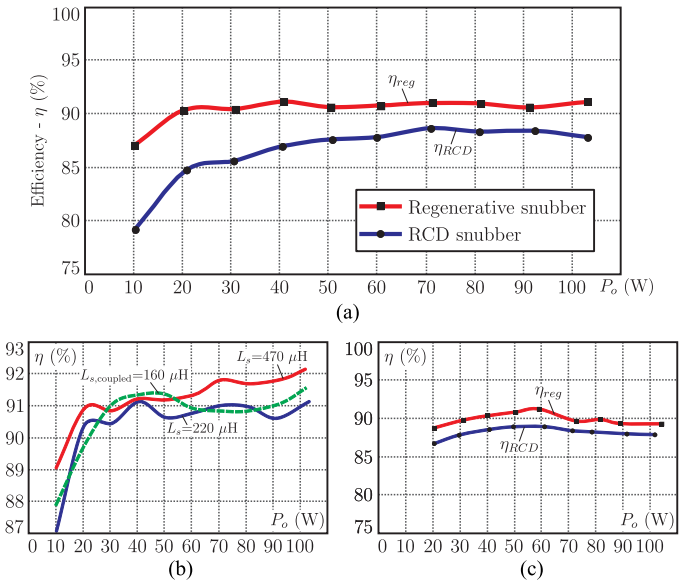

Fig. 17. Experimental efficiency curves: (a) Efficiency comparison between the RCD snubber and the proposed regenerative snubber for DCM operation. (b) Efficiency curves for two different snubber inductance values and snubber coupled inductors (dashed line) in DCM. (c) Efficiency comparison between the RCD snubber and the proposed regenerative snubber for CCM operation.

The last efficiency curve, Fig. 17(c) shows the same comparison as in Fig. 17(a), but for the CCM operation. The results are also better when the regenerative snubber is used (around 2%). The improvement is smaller than for DCM because the converter was first developed and optimized for this mode and later adapted for CCM. Nevertheless, the use of the proposed regenerative snubber cell for CCM is also validated and can be an option.

VII. Conclusion

A regenerative snubber, as applied to SEPIC converters in both operational modes, is presented and compared to a dissipative snubber (RCD). The complete qualitative analysis is given for DCM and extended to CCM operation. Based on a specification example, the snubber cells were designed and experimentally tested in order to prove the concept. Additionally, the results are compared with RCD snubber to validated the efficiency improvements. Analytical descriptions and design guidelines are presented for both snubbers. All the results are in quite good agreement with the expectations, proving the concept and the design methodology of the RCD and regenerative snubbers. The improvement in the converter efficiency when operating in nominal power is around 3% for DCM and 2% for CCM when compared to an RCD snubber. For applications with larger leakage inductances, such as isolated high voltage supplies, the proposed snubber is expected to provide even more efficiency improvement. The snubbers inductors can also be coupled, as experimentally demonstrated, reducing the component count and it may bring extra advantages. This should be investigated in a further work. Therefore, this regenerative snubber is an attractive solution for improving the efficiency of isolated SEPICs.

References

[1] C. Canesin and I. Barbi, "A unity power factor multiple isolated outputs switching mode power supply using a single switch," in *Proc. 60th Annu. Appl. Power Electron. Conf. Expo.*, Mar. 1991, pp. 430–436.

[2] D. Lyrio Simonetti, J. Sebastian, and J. Uceda, "The discontinuous conduction mode SEPIC and CUK power factor preregulators: Analysis and design," *IEEE Trans. Ind. Electron.*, vol. 44, no. 5, pp. 630–637, Oct. 1997.

[3] P. de Melo, R. Gules, E. Romaneli, and R. Annunziato, "A modified SEPIC converter for high-power-factor rectifier and universal input voltage applications," *IEEE Trans. Power Electron.*, vol. 25, no. 2, pp. 310–321, Feb. 2010.

[4] R. Ayyanar, N. Mohan, and J. Sun, "Single-stage three-phase power-factor-correction circuit using three isolated single-phase SEPIC converters operating in CCM," in *Proc. IEEE 31st Annu. Power Electron. Spec. Conf.*, 2000, vol. 1, pp. 353–358.

[5] G. Tibola and I. Barbi, "Isolated three-phase high power factor rectifier based on the SEPIC converter operating in discontinuous conduction mode," *IEEE Trans. Power Electron.*, vol. 28, no. 11, pp. 4962–4969, Nov. 2013.

[6] B.-R. Lin and C.-C. Chen, "Soft switching isolated SEPIC converter with the buck-boost type of active clamp," in *Proc. 2nd IEEE Int. Conf. Ind. Electron. Appl.*, May 2007, pp. 1232–1237.

[7] A. Ghasemi, E. Adib, and M. Mohammadi, "A new isolated SEPIC converter with coupled inductors for photovoltaic applications," in *Proc. 19th Iranian Conf. Elect. Eng.*, May 2011, pp. 1–5.

[8] B.-R. Lin, J.-J. Chen, and J.-F. Wan, "Active clamp SEPIC converter with power factor correction," in *Proc. 33rd Annu. Conf. IEEE Ind. Electron. Soc.*, Nov. 2007, pp. 1989–1994.

[9] P. Athalye, D. Maksimovic, and R. Erickson, "Improving efficiency of the active-clamped SEPIC rectifier at high line frequencies," in *Proc. 20th Annu. IEEE Appl. Power Electron. Conf. Expo.*, Mar. 2005, vol. 2, pp. 1152–1157.

[10] A. Abramovitz, J. Yao, and K. Smedley, "Derivation of a family of high step-up tapped inductor SEPIC converters," *IET Electron. Lett.*, vol. 50, no. 22, pp. 1626–1628, 2014.

[11] J. Yao, A. Abramovitz, and K. Smedley, "Analysis and design of charge pump-assisted high step-up tapped inductor SEPIC converter with an "inductor-less" regenerative snubber," *IEEE Trans. Power Electron.*, vol. 30, no. 10, pp. 5565–5580, Oct. 2015.

[12] V. Bonfa, P. Menegaz, J. Vieira, and D. Simonetti, "Multiple alternatives of regenerative snubber applied to SEPIC and CUK converters," in *Proc. IEEE 28th Annu. Conf. Ind. Electron. Soc.*, Nov. 2002, vol. 1, pp. 123–128.

[13] I. Burgardt, E. A. Junior, C. H. I. Font, and C. B. Nascimento, "Dimmable flicker-free power LEDs lighting system based on a SEPIC rectifier using a regenerative snubber," *IET Power Electron.*, vol. 9, no. 5, pp. 891–899, 2016.

[14] M. Domb, R. Redl, and N. O. Sokal, "Nondissipative turn-off snubber alleviates switching power dissipation, second-breakdown stress and VCE overshoot: Analysis, design procedure and experimental verification," in *Proc. 1982 IEEE Power Electron. Spec. Conf.*, Jun. 1982, pp. 445–454.

[15] T. Ninomiya, T. Tanaka, and K. Harada, "Analysis and optimization of a nondissipative LC turn-off snubber," *IEEE Trans. Power Electron.*, vol. 3, no. 2, pp. 147–156, Apr. 1988.

[16] R. Petkov and L. Hobson, "Analysis and optimisation of a flyback convertor with a nondissipative snubber," *Inst. Electr. Eng. Proc.-Electr. Power Appl.*, vol. 142, no. 1, pp. 35–42, Jan. 1995.

[17] T.-H. Hai, "A novel integrated non-dissipative snubber for flyback converter," in *Proc. IEEE Int. Conf. Syst. Signals*, Jun. 2005, pp. 66–71.

[18] A. Abramovitz, C. S. Liao, and K. Smedley, "State-plane analysis of regenerative snubber for flyback converters," *IEEE Trans. Power Electron.*, vol. 28, no. 11, pp. 5323–5332, Nov. 2013.

[19] C. Vartak, A. Abramovitz, and K. M. Smedley, "Analysis and design of energy regenerative snubber for transformer isolated converters," *IEEE Trans. Power Electron.*, vol. 29, no. 11, pp. 6030–6040, Nov. 2014.

[20] T. Meng, H. Ben, D. Wang, and J. Song, "Novel passive snubber suitable for three-phase single-stage PFC based on an isolated full-bridge boost topology," *JPE J. Power Electron.*, vol. 11, no. 3, pp. 264–270, May 2011.

[21] T. Meng, H. Ben, L. Zhu, and G. Wei, "Improved passive snubbers suitable for single-phase isolated full-bridge boost power factor correction converter," *IET Power Electron.*, vol. 7, no. 2, pp. 279–288, Feb. 2014.

[22] G. Tibola, E. Lemmen, and J. Duarte, "Passive regenerative snubber cell applied to isolated DCM SEPIC converter," in *Proc. IEEE 8th Int. Power Electron. Motion Control Conf.*, May 2016, pp. 2779–2786.

[23] G. Tibola, E. Lemmen, and J. Duarte, "Comparison between dissipative snubber and passive regenerative snubber cells as applied to isolated DCM SEPIC converters," in *Proc. 18th Eur. Conf. Power Electron. Appl.*, Sep. 2016, pp. 1–10.
[24] L. De Vicuna, F. Guinjoan, J. Majo, and L. Martinez, "Discontinuous conduction mode in the SEPIC converter," in *Proc. Mediterranean Electrotech. Conf.*, Apr. 1989, pp. 38–42.

Gabriel Tibola (M'15) was born in Coronel Freitas, Brazil, in 1981. He received the B.S., M.S., and Ph.D. degrees in electrical engineering from the Federal University of Santa Catarina, Florianópolis, Brazil, in 2006, 2009, and 2013, respectively.

Since 2013, he has been a Postdoctoral Researcher Engineer in the Electromechanics and Power Electronics group, Eindhoven University of Technology, Eindhoven, The Netherlands. His research interests include ac–dc and dc–dc power converters, power factor correction, and sustainable energy sources.

Erik Lemmen (S'13) received the B.Eng. degree *cum laude* in electrical engineering from the Fontys University of Applied Sciences, Eindhoven, The Netherlands, in 2009 and the M.Sc. degree in power electronics from the Eindhoven University of Technology, Eindhoven, The Netherlands, in 2013. Since 2013, he has been working toward the Ph.D. degree in the group of Electromechanics and Power Electronics, Eindhoven University of Technology.

His research interests include multilevel topologies, redundancy in power converters, and modular converter structures.

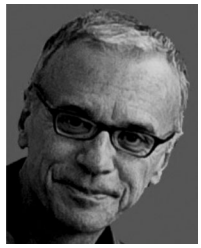

Jorge L. Duarte (M'99) received the M.Sc. degree in electrical engineering from Federal University of Rio de Janeiro, Rio de Janeiro, Brazil, in 1980 and the Dr. Ing. degree from the Institute National Polytechnique de Lorraine, Nancy, France, in 1985.

In 1989, he was appointed a Research Engineer at Philips Lighting Central Development Laboratory. Since 1990, he has been a member of the academic staff in the Electromechanics and Power Electronics Group, Eindhoven University of Technology, Eindhoven, The Netherlands. Since October 2000, he has been a Consultant Engineer on a regular basis at high-tech industries around Eindhoven. His teaching and research interests include modeling, simulation, and design optimization of power electronic systems.

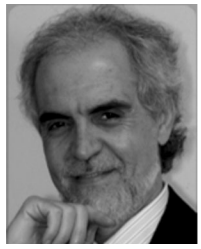

Ivo Barbi (F'11) was born in Gaspar, Brazil, in 1949. He received the B.S. and M.S. degrees in electrical engineering from the Federal University of Santa Catarina, Florianópolis, Brazil, in 1973 and 1976, respectively, and the Dr. Ing. degree in electrical engineering from the Institut National Polytechnique de Toulouse, Toulouse, France, in 1979.

He founded the Brazilian Power Electronics Society (SOBRAEP) and the Brazilian Power Electronics Conference in 1990, and the Brazilian Power Electronics and Renewable Energy Institute in 2016.

Prof. Barbi is an Associate Editor of the IEEE TRANSACTIONS ON POWER ELECTRONICS and the *IET Electronics Letters*, the President of the Brazilian Power Electronics and Renewable Energy Institute, a Researcher at the Solar Energy Research Center, and a Professor of electrical engineering at Federal University of Santa Catarina.